CHARACTERIZATION OF SECOND HARMONIC AFTERBURNER RADIATION AT THE LCLS*

H.-D. Nuhn#, F.-J. Decker, Y. Ding, P. Emma, A. Fisher, J. Frisch, Z. Huang, R. Iverson, J. Krzywinski, H. Loos, Y. Levashov, H. Loos, M. Messerschmidt, T. Smith, D.F. Ratner, J.L. Turner, J.J. Welch, Z.R. Wolf, J. Wu,
SLAC National Accelerator Laboratory, Stanford, CA 94309, U.S.A.

Abstract

During commissioning of the Linac Coherent Light Source (LCLS) x-ray Free Electron Laser (FEL) at the SLAC National Accelerator Laboratory it was shown that saturation lengths much shorter than the installed length of the undulator line can routinely be achieved [1]. This frees undulator segments that can be used to provide enhanced spectral properties and at the same time, test the concept of FEL Afterburners.

In December 2009 a project was initiated to convert undulator segments at the down-beam end of the undulator line into Second Harmonic Afterburners (SHAB) to enhance LCLS radiation levels in the 10 – 20 keV energy range. This is being accomplished by replacement of gap-shims increasing the fixed gaps from 6.8 mm to 9.9 mm, which reduces their K values from 3.50 to 2.25 and makes the segments resonant at the second harmonic of the upstream unmodified undulators.

This paper reports experimental results of the commissioning of the SHAB extension to LCLS.

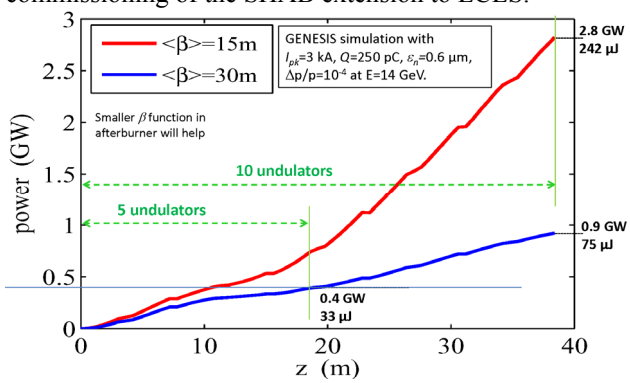

Figure 1: LCLS SHAB performance prediction at 14 GeV based on FEL simulations using GENESIS 1.3 for $<\beta_{x,y}>$=30 m (standard LCLS undulator lattice) and $<\beta_{x,y}>$=15 m. The latter is beyond the present capability of the quadrupole system, which is limited to $<\beta_{x,y}>$~22 m at 14 GeV.

INTRODUCTION

In a SASE FEL, strong bunching at the fundamental wavelength can drive substantial nonlinear harmonic bunching [2] at both odd and even harmonics. A second undulator may be used to produce FEL quality radiation from this micro-bunched beam. That second undulator can be tuned to the fundamental or to one of the harmonics [3] and can have polarization properties different from the first undulator. The second undulator, used in this configuration, is now called an Afterburner. Fundamental and second harmonic Afterburners are planned for the XFEL project and for upgrades to the LCLS.

This paper describes a test of the Afterburner concept at the Linac Coherent Light Source (LCLS), using a Second Harmonic Afterburner (SHAB), as proposed in [4], as an example of an Afterburner type configuration. The expected performance increase as estimated by GENESIS 1.3 [5] is shown in Figure 1. The prediction for the five SHAB case (as described in this paper) is 0.4 GW at E =14 GeV (fundamental and 2nd harmonic photon energy at 8.7 keV and 17.4 keV, respectively) corresponding to 33 μJ for a flat-top beam of Q = 250 pC and I_{pk} = 3 kA (corresponding to 83 fs fwhm).

GAP INCREASE AND TUNING

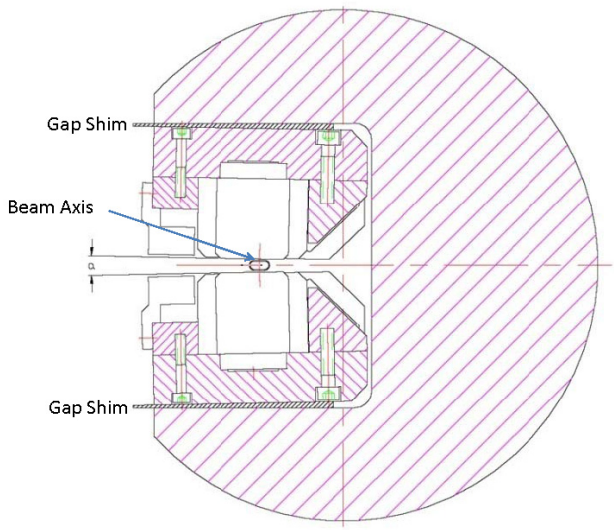

Figure 2: Cross section of an LCLS undulator segment (as designed by the Argonne National Laboratory [6]). The thickness of the tapered gap shims was reduced from about 2 mm to about 0.45 mm to make some of the Undulator Segments resonant to the 2nd harmonic of the unmodified undulators.

The LCLS uses 33 fixed-gap undulator segments with a nominal strength of K_1 = 3.5 and a period λ_u = 0.03 m [7]. For the work discussed in this paper, the gaps of the last five of these undulator segments have been increased

* Work by U.S. Department of Energy contract DE-AC02-76SF00515
# nuhn@slac.stanford.edu

from 6.8 mm to 9.9 mm (see **Figure 2**) to make them resonant at the second harmonic of the regular undulators, at $K_2 = \sqrt{K_1^2/2 - 1} = 2.25$.

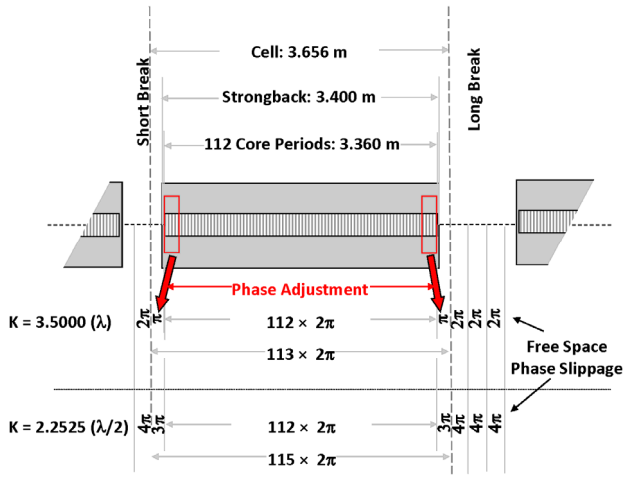

Figure 3: LCLS Undulator Phase Scheme: For the regular strength, the Cell length of 3.656 m is defined as the distance over which the phase slippage is exactly 113×2π rad. The transition between the 112 core period and the Cell boundary is tuned to be π rad for each undulator. The Break length is designed to be a multiple of $\lambda_u\left(K_1^2/2+1\right)$ for which 2π rad phase slippage occurs in free space. With the larger gap, the transition phase is adjusted to be 3π rad .

The LCLS undulator segments are separated from each other by short and long break sections to allow for installation of quadrupoles, BPMs etc. The sizes of these break sections have been designed to provide the correct phase slippage for the nominal *K* parameter. Phase shims were added to the undulator end sections (outer 4 poles) to ensure this phase relation to stay correct for the larger gap devices (see Figure 3).

SETUP

In order to achieve optimum FEL performance, each SHAB test session was started with one or more iteration of the Beam Based Alignment (BBA) procedure, while all 33 undulator segments were inserted. The SHABs were then removed (moved to $x = 80$ mm) and the electron beam energy was adjusted to tune the weak 2nd harmonic of the standard undulators to the correct photon energy for the selected detector.

Three different detector setups, each at a different photon energy, were used (See Figure **4** for the relative locationof the detector components):

1. K-Mono [8]: This monochromator has a 1-eV wide pass band at a photon energy of 8.192 keV and its harmonics. Due to this very narrow bandwidth, it is difficult to align, but was successfully used to measure the *K* response curve of individual SHABs.
2. Zr/Si Foil: A combination of Zr and Si foils, installed about 48 m after the end of U33 (in the so-called ST-0 can) has been used to remove the fundamental radiation component produced by the regular undulator segments.

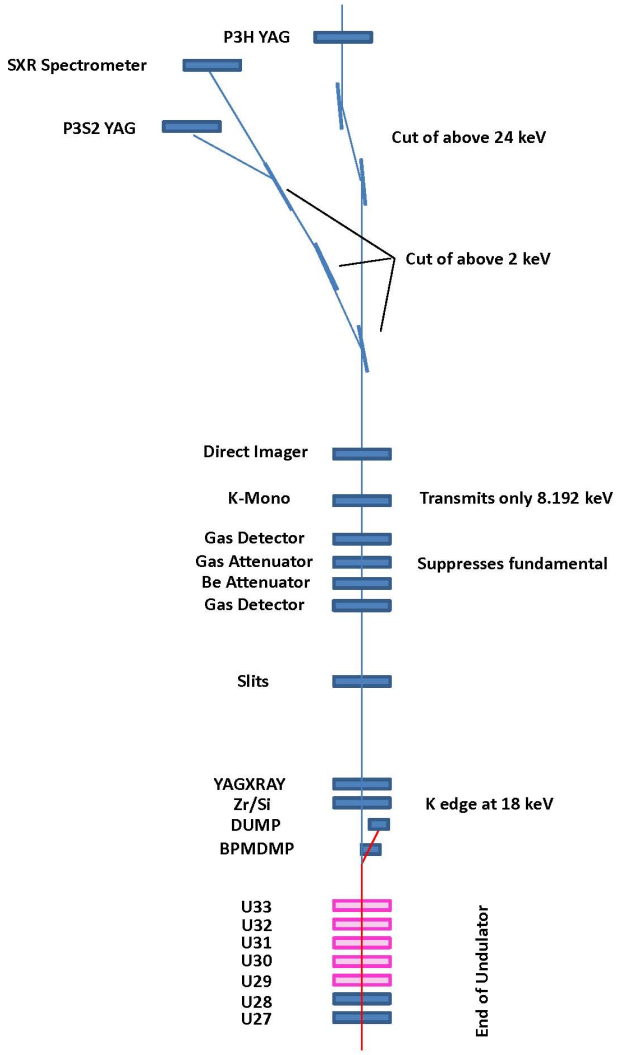

Figure 4: Sketch of the "FEE" diagnostics suite at LCLS used to detect the SHAB signal.

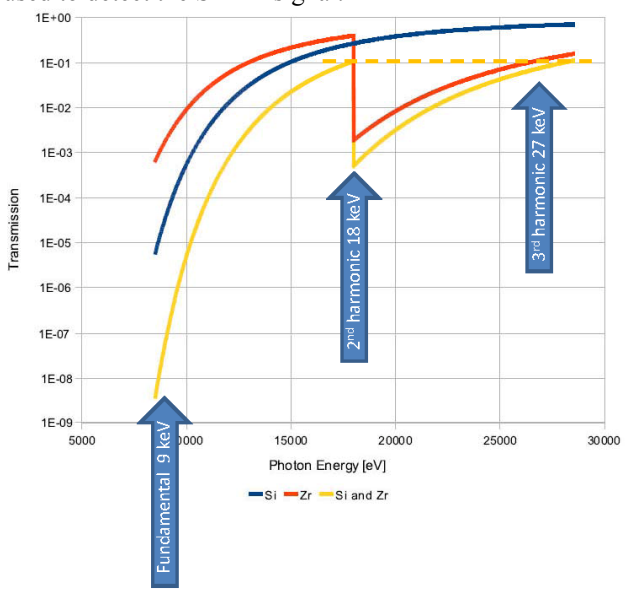

Figure 5: Zr and Si x-ray absorption functions.

As can be seen in Figure 5, when operating the electron beam energy at 14.2 GeV to position the 2nd harmonic close to the Zr K edge at 18 keV, the fundamental at 9 keV is attenuated by 7 orders of magnitude. The filtered pulse can be observed with a YAG screen (YAGXRAY) located right after the foil package. But it will be contaminated with the 3rd harmonic component at 27 keV, which the Zr/Si does not sufficiently attenuate. A pair of hard x-ray mirrors with a cut-off around 24 keV can be used to isolate the 2nd harmonic on another YAG screen (P3H). Insufficient mirror dimensions, saturation effects in the YAG and mirror alignment problems make this option less attractive.

3. SXR YAG: The third method relies on the energy dependent absorption in the N_2 gas attenuators while operating at a SHAB energy of about 1.8 keV. Again, the third harmonic component needs to be removed separately. In this case, this is done with three SXR mirrors with a cut-off above 2.2 keV [9].

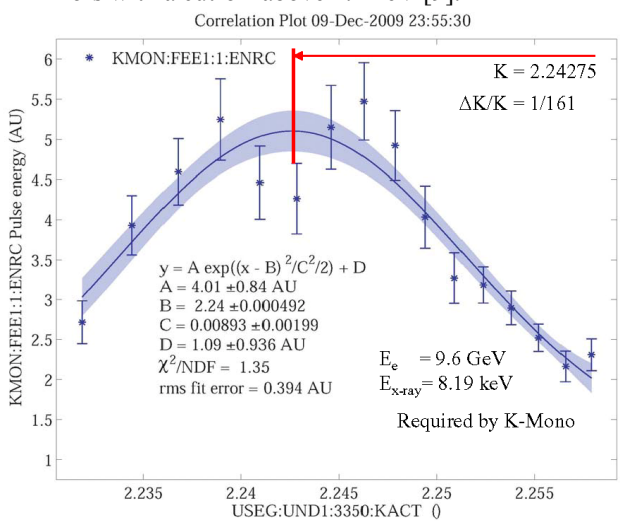

Figure 6: SHAB signal at 8.912 eV from U33 with 32 bunching undulators installed (E = 9.63 GeV).

RESULTS

The first test was carried out in December 2009 with the first SHAB installed in slot U33. Figure 6 shows a scan of SHAB K values (x position scan making use of the pole face canting in the LCLS undulator segments) versus the integrated intensity of the signal through the narrow K-Mono bandwidth (method 1). The result is fitted with a Gaussian function which provides an estimate for the intensity increase compared to the 2nd harmonic of the 28 regular (upstream) undulator segments. The rms width of the resonance is a bit smaller than $1/N_u$ while the K value of the peak is close to the expected value.

Using the Zr/Si filter, as described in detector setup (2) the amount of 2nd harmonic can be verified at 18 keV (Figure 7) at E = 14.232 GeV. Background subtraction effectively removed non-beam background. Above-K-edge intensity from the 3rd harmonic and leakage from energy tails are quite low.

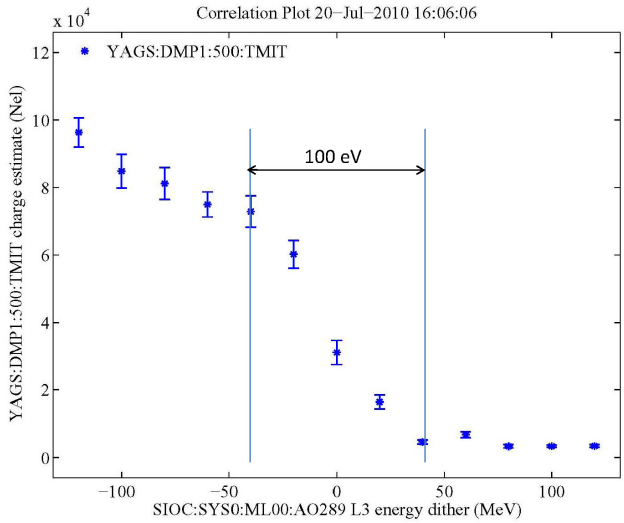

Figure 7: SHAB output transmitted through the Zr/Si filter and observed on YAGXRAY while electron energy is scanned to move photon energy across the Zr K edge at 18,000 eV. The horizontal axis is in units of electron energy (the corresponding photon energy range of 100 eV is marked). The vertical axis is the total pixel count on the YAG screen.

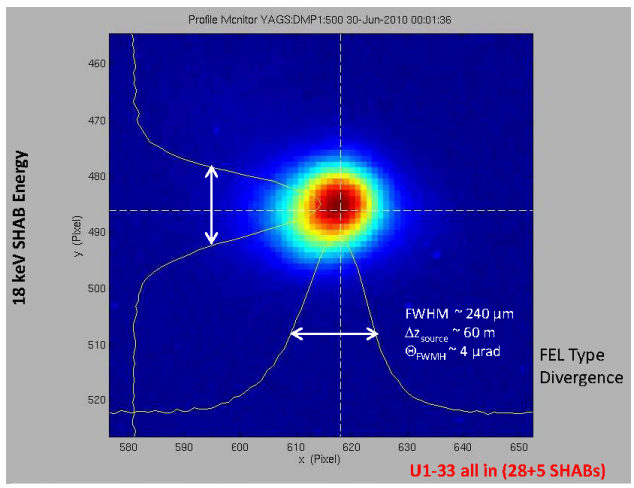

Figure 8: Image of SHAB beam on YAGXRAY located right after the Zr/Si foil. The estimated divergence of about 4 µrad underlines the FEL quality of the beam.

Based on this result, the image at the following YAG screen (Figure 8) should be mostly 2nd harmonic. One of its characteristics is its small fwhm size of about 16 pixels or 240 µm, which, with the source point location estimated to be about 60 m upstream, translates to the FEL quality fwhm beam divergence of 4 µrad.

At 1.8 keV SHAB energy (E = 4.5 GeV), the effect of gain taper on SHAB performance was studied. The measurement started with a constant gradient taper of $\Delta K/K/\Delta L$ = -0.0034%/m for the regular undulator segments and for the SHABs. Increasing the absolute value of the taper gradient in the SHABs (**Figure 9**) increases the SHAB output intensity by up to a factor 2

(Figure 10). The optimum occurs at a total gradient of $\Delta K/K/\Delta L$ = -0.0136%/m.. This dependence on tapering indicates that SHAB radiation is indeed based on micro-bunching. In **Figure** 9, the K values of the SHABs are plotted as $\sqrt{2(K^2+1)}$, called "equivalent K" values.

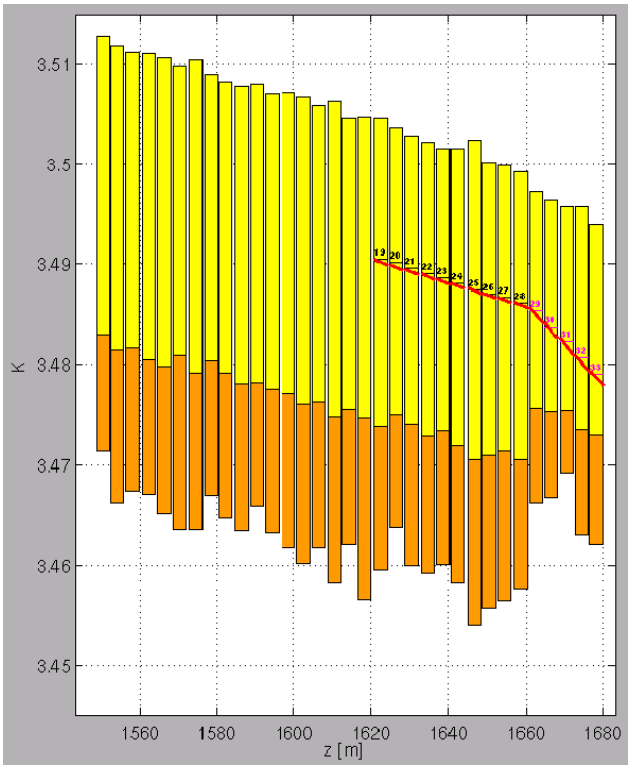

Figure 9: Taper Settings: K versus z location. Black/Magenta horizontal bars; K values of regular/ "equivalent K" (see text) values of SHAB segments. yellow/orange blocks standard/extended segment K tuning ranges.

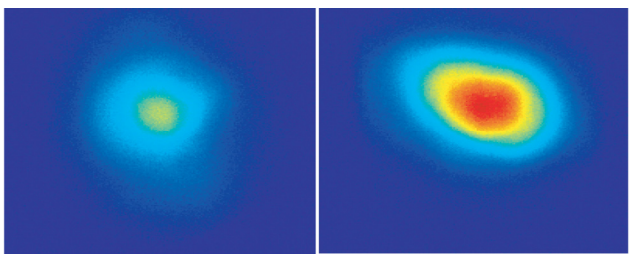

Figure 10: The two YAG images show the SHAB beam before (left) and after (right) a taper of $\Delta K/K$ = -0.01%/m is added along the five SHABs. The SHAB intensity at 1.8 keV doubles due to this added taper.

Using detector setup (3), the kick method (see caption in Figure 11 for explanation) was used to determine the energy gain in each of the SHAB undulators at the optimum taper. The first three data points (circles) in Figure 11 are from regular undulators, the last five are the SHABs, which produce a steady increase consistent with the predictions in Figure 1 and Figure 12. Note: the simulation shown in Figure 1 predicts further increase in SHAB intensity if more SHABs are added, even though the intensity appears to taper off towards the fifth SHAB.

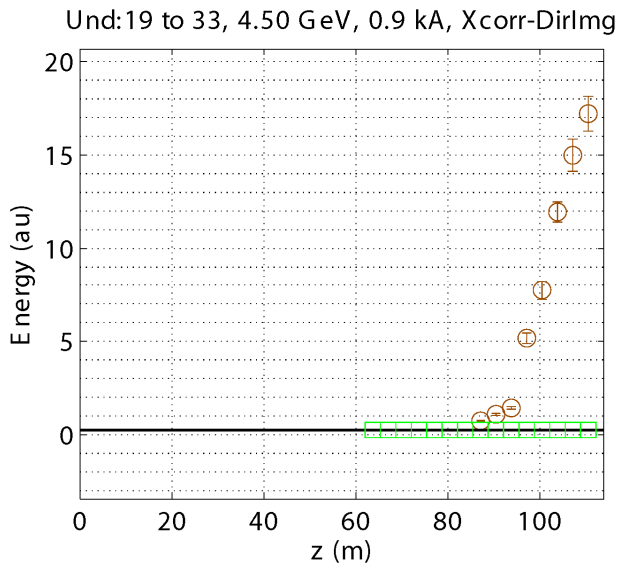

Figure 11: X-ray pulse energy (circles and error bars) versus undulator position. For each data point, the trajectory was kicked in the horizontal plane to destroy micro-bunching and/or FEL gain down stream. The green boxes stand for the 15 undulators segments that were in use (rolled-in) during the measurement.

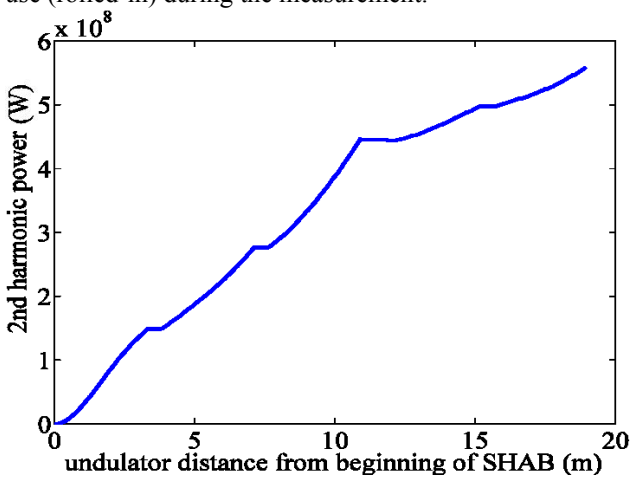

Figure 12: Prediction of SHAB output at 1.8 keV after nine regular undulators saturated just upstream. The data does not contain any of the radiation produced upstream of the SHAB. (GENESIS 1.3 simulation: with I_{pk} = 1 kA, ε_n = 0.6 µm, $\Delta p/p = 10^{-4}$ at E = 4.5 GeV.) The maximum power of about 0.55 GW corresponds to 0.12 mJ pulse energy for the 250 fs long flat-top pulse

This tapering off of SHAB output with SHAB number is possibly due to a debunching effect at the beginning of the SHAB line due to the large energy spread of the beam after coming out of saturation and the $R_{56} \sim -2\, N_u\, \lambda_r$ of the SHAB undulators (N_u being the number of undulator periods and λ_r the resonant wavelength). Together these parameters would debunch the beam after only 2 SHABs if longitudinal beam dynamics in the SHABs would not counteract the process. The ratio of energy spread to bunching amplitude can be improved by inserting a dispersive section between the two undulators, which

would act on the pre-saturated bunch (similar to the HGHG scheme [10]). This method was proposed in [11] but has not been used for this paper.

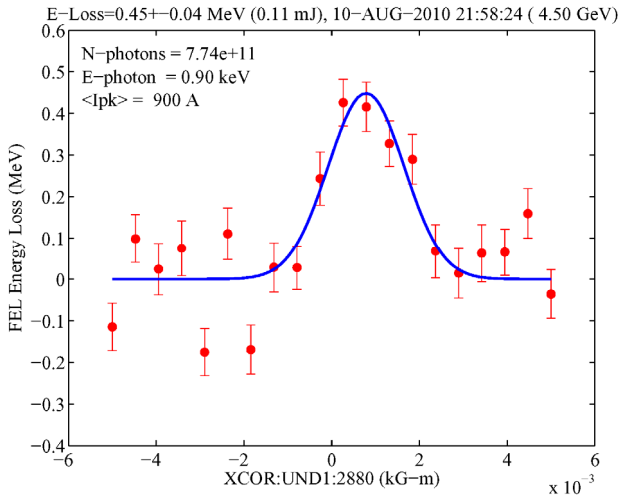

Figure 13: Eloss scan: The corrector just upstream of the first SHAB (U29) is scanned and plotted versus the average energy of the electron beam arriving at the electron beam dump, as measured with the Dump BPM, located in a high dispersion region.

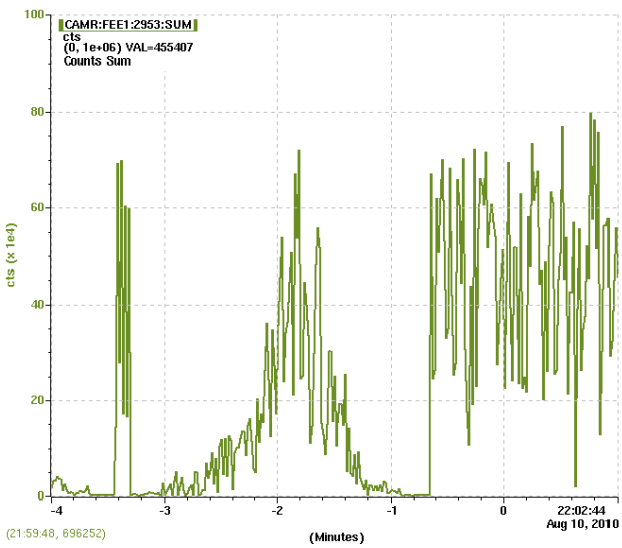

Figure 14: Gas detector signal during the eloss scan procedure shows the dependence of x-ray pulse intensity on electron beam trajectory in the SHAB line

Calibrating the energy axis of Figure 11 is not straightforward due to the lack of absolute calorimeters at LCLS. We made use of a method normally used for estimating the energy content of LCLS x-ray pulses, i.e. the “eloss scan”. The eloss scan, in its normal use, kicks the electron beam at the first undulator segment to generate large amplitude betatron oscillations along the undulator, which suppresses FEL gain. The scan uses a large, bi-polar kick range and applies a Gaussian fit to the resulting average beam position as measured at high dispersion region on the Dump BPM. In the present case (Figure 11) we started with a slight variation of that scan, i.e., we selected a corrector just upstream of the first SHAB to kick the beam (see Figure 13). The resulting measurement data is just barely above the noise and yields a value of 0.11 mJ of total SHAB intensity. The x-ray pulse intensity during the SHAB scan is shown in Figure 14. The strong correlation between corrector strength (i..e. electron beam trajectory) and x-ray beam intensity confirms that the SHAB radiation is based on micro-bunching.

In an attempt to improve the signal-to-noise ratio of the scan, a combination of two full line scans (i.e. scans that turn off FEL gain in both the regular undulator and the SHABs) was used. The second scan used a second, fixed, corrector in front of the first SHAB to deactivate the SHABs during the scan (Figure 15). The difference of the 0.55 mJ from scan 1 and the 0.46 mJ from scan 2 is close (0.08 mJ) to the previous result and supports a value of about 0.1 mJ in agreement with simulation.

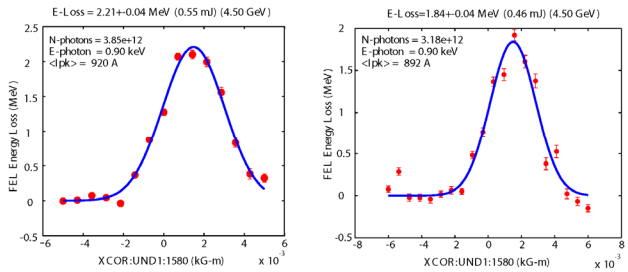

Figure 15: Eloss scan, similar to Figure 13 but using a corrector just upstream of the first regular inserted undulator (U16). For the right hand side figure the corrector in front of the first SHAB (U29) is turned on to permanently deactivate the SHABs.

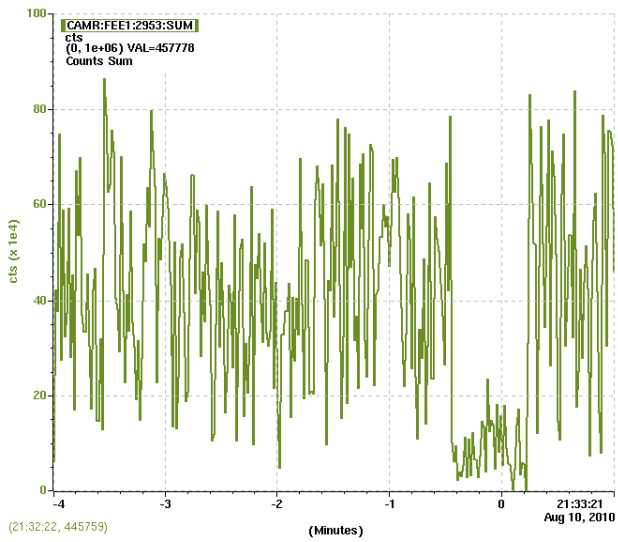

Figure 16: Gas Detector Signal showing SHAB output while Laser Heater is deactivated (low intensity section).

The LCLS uses a Laser-Heater [12] to reduce degradation in FEL performance from coherent synchrotron radiation in the bunch compressors and dog-legs. The Laser-Heater system modulates the energy of the 135-MeV electron

bunch with an IR laser beam in a short undulator enclosed within a four-dipole chicane.

The IR laser beam of the Laser Heater systems is normally set to about 7 – 10 μJ. In order to find out if SHAB output is sensitive to the Laser Heater, we temporarily deactivated the Laser Heater by blocking the IR laser from reaching the Laser Heater undulator. Figure 16 shows the SHAB output as seen by the Gas Detector during the time while the Laser Heater was deactivated. The IR laser was blocked during the time interval -0.5 minutes to 0.2 minutes in the time scale of the figure. The significant reduction in output power demonstrates both the dependence of SHAB performance on electron beam quality and the importance of the Laser Heater system for SHAB operation, in general.

SUMMARY

The five SHABs tested, generate ~0.1 mJ of 2nd harmonic power at 1.8 keV. At 18 keV (14.2 GeV electron energy) the pulse intensity calibration is uncertain and the SHAB intensity may be substantially lower than at 1.8 keV. Nevertheless, at 18 keV, the relative intensity exceeds that of the 3rd FEL harmonic at the same photon energy (but lower electron energy, i.e., 11.6 GeV) of the normal undulator segments by at least a factor of 2. This factor is expected to increase to 10 or larger if more SHABs are installed and if the beta-function is reduced. SHAB power increases over all five SHABs in reasonable agreement with simulations. The signal is sensitive to the Laser Heater setting. The experimental results presented in this paper show that a Second Harmonic Afterburner can be used to significantly increase the LCLS x-ray pulse intensity in the 10 – 20 keV range. More SHABs are ready to be installed. If and when they will be installed depends on user needs.

ACKNOWLEDGEMENTS

It is a pleasure to acknowledge contributions by many SLAC colleagues, especially the operations team.

REFERENCE

[1] P. Emma, R. Akre, J. Arthur, R. Bionta, C. Bostedt, J. Bozek, A. Brachmann, P. Bucksbaum, R. Coffee, F.-J. Decker, Y. Ding, D. Dowell, S. Edstrom, A. Fisher, J. Frisch, S. Gilevich, J. Hastings, G. Hays, Ph. Hering, Z. Huang, R. Iverson, H. Loos, M. Messerschmidt, A. Miahnahri, S. Moeller, H.-D. Nuhn, G. Pile, D. Ratner, J. Rzepiela, D. Schultz, T. Smith, P. Stefan, H. Tompkins, J. Turner, J.Welch, W. White, J. Wu, G. Yocky, J. Galayda "First Lasing and Operation of an Angstrom-Wavelength Free-Electron Laser", *nature photonics*. DOI: 10.1038/NPHOTON.2010.176 (2010)

[2] R. Bonifacio, L. De Salvo Souza, P. Perini, E.T. Scharlemann, "Generation of XUV Light by Resonant Frequency Tripling in a Two-Wiggler FEL Amplifier," *Nucl. Instr. Meth. A* ***296*** (1990), pp. 787 – 790

[3] W.M. Fawley, H.-D. Nuhn, R. Bonifacio, E.T. Scharlemann, "Merits of a Sub-Harmonic Approach to a Single-Pass 1.5-Å FEL" *in Proceedings of the 1995 Particle Accelerator Conference*, p. 219

[4] Z. Huang, S. Reiche, "Generation of GW-level, sub-Angstrom Radiation in the LCLS using a Second-Harmonic Radiator" *in Proceedings of the 2004 FEL Conference (FEL 04)*, pp. 201-204

[5] S. Reiche, "GENESIS 1.3: A Fully 3D Time-Dependent FEL Simulation Code," *Nucl. Instr. and Meth. A* ***429*** (199), pp. 243 – 248.

[6] G. Pile, J.L. Bailey, T. Barsz, W. Berg, J.T. Collins, P.K. Den Hartog, H.W. Friedsam, M.S. Jaski, S.-H. Lee, R.M. Lill, E.R. Moog, J.W. Morgan, S. Sasaki, S.E. Shoaf, L. Skubal, S.J. Stein, W.F. Toter, E. Trakhtenberg, I. Vasserman, D.R. Walters, M. White, G.E. Wiemerslage, J.Z. Xu, B.X. Yang, H.-D. Nuhn, "Design and Construction of the Linac Coherent Light Source (LCLS) Undulator System," *in Proceedings of FEL08,* Gyeongju, Korea, pp. 460 – 466. (2008)

[7] H.-D. Nuhn, "LCLS Undulator commissioning, alignment, and performance", *in Proceedings of the 2009 FEL Conference (FEL 09)* , pp. 714 – 721.

[8] J.J. Welch, A. Brachmann, F.-J. Decker, Y. Ding, P. Emma, A. Fisher, J. Frisch, Z. Huang, R. Iverson, H. Loos, H.-D.Nuhn, P.Stefan, D. Ratner, J. Turner, J. Wu, D. Xiang, R. Bionta, H. Sinn, „Undulator *K*-Parameter Measurements at LCLS," *in Proceedings of FEL09, Liverpool*, UK, pp. 730 – 733. (2009)

[9] D. Ratner, A. Brachmann, F.J. Decker, D. Dowell, P. Emma, J. Frisch, Z. Huang, R. Iveson, J. Krzywinski, H. Loos, M. Messerschmidt, H.-D. Nuhn, T. Smith, J. Turner, J. Welch, W. White, J. Wu, R. Bionta, „Second and Third Harmonic Measurements at the Linach Coherent Light Source," *these Proceedings.*

[10] L.H. Yu, "Generation of Intense UV Radiation by Subharmonically Seeded Single-Pass Free-Electron Lasers," *Phys. Rev.* A **44**, 5178 – 5193 (1991)

[11] J. Feldhaus, M. Körfer, T. Möller, J. Pflüger, E.L. Saldin, E.A. Schneidmiller, M.V. Yurkov, "Efficient Frequency Doubler for the soft X-ray SASE FEL at the TESLA Test Facility," *Nucl. Instr. and Meth. A* ***528*** (2004), pp. 471 – 475.

[12] P. Emma, R.F. Boyce, A. Brachmann, R. Carr, F.-J. Decker, Y. Ding, D. Dowell, S. Edstrom, J. Frisch, S. Gilevich, G. Hays, Ph. Hering, Z. Huang, R. Iverrson, Y. Levashov, H. Loos, A. Miahnahri, H.-D. Nuhn, B. Poling, D. Ratner, S.Spampinati, J. Turner, J. Welch, W. White, Z. Wolf, J. Wu, ", First Results of the LCLS Laser-Heater System" *in Proceedings of PAC09, Vancouver, BC, Canada* (2009).